Applied Materials Today 45 (2025) 102831

Contents lists available at ScienceDirect

Applied Materials Today

journal homepage: www.elsevier.com/locate/apmt

Multitasking carbohydrate-functionalized 2D germanane with implanted supramolecular stereodiscrimination ability

Yiming Lei [1], Ángel Campos-Lendínez [1], Xavier Sala, Jordi García-Antón, Jose Muñoz [*]

Departament de Química, Universitat Autònoma de Barcelona, Cerdanyola del Vallès, Barcelona, 08193, Spain

ARTICLE INFO

Keywords:
Chirality
Cyclodextrin
Host–guest
Germanene
2D materials

ABSTRACT

Due to their promising photoelectronic features, 2D–Germanane (2D–GeH) and their ligand-terminated derivatives (2D–GeR) have garnered significant attention in the Materials Science community. To date, the synthesis of 2D–GeR relies on a tedious topochemical reaction, a fact that not only limits the variety of R ligands that can be incorporated but also restricts their stability and applicability. Herein, a highly stable carbohydrate-based 2D germanane derivative with built-in stereodiscrimination ability has been synthesized *via* a direct covalent immobilization of a cyclic oligosaccharide selector (*viz.* thiolated β-cyclodextrin, CD–SH) onto 2D–GeH. By taking advantage of the CD affinity to accommodate different stereoisomers through supramolecular host–guest interactions, the multitasking activity of the resulting 2D–GeCD has been explored for the selective discrimination of enantiomers and diastereomers. Overall, this chemical approach is general and opens up the development of multitasking 2D–GeR derivatives by incorporating supramolecular features, which can be easily extended to a wide range of bio-molecules by tailoring the stereometric host–guest encapsulation.

1. Introduction

Carbohydrates are abundant biomolecules that play a crucial role in supramolecular chemistry owing to their strong tendency to form dynamic host–guest interactions [1]. The appealing chemistry of carbohydrates to form a large number of hydrogen bonds has led to the development of a wide variety of carbohydrate-based nanomaterials for well-distinguished applications [2–5], ranging from biosensing to drug delivery and molecular switches [6–9]. In particular, cyclodextrins (CDs) —cyclic oligosaccharides composed of glucose units— have been widely explored as chiral selectors in the pharmaceutical industry due to their ability to form stable supramolecular host–guest complexes in aqueous media with a broad range of small guest targets [10]. From a life science point of view, chiral discrimination is of essential importance since the enantiomeric forms of chiral drugs usually show different metabolic and pharmacological effects in biological systems. In addition, CDs are ideal cargo vehicles that can modulate delivery by taking advantage of their different affinity towards isomeric forms, making them very promising for diastereospecific drug transport and release [11].

While graphene has long dominated the field of 2D materials, the Materials Science community is currently focused on exploring emerging 2D monoelemental materials (known as 2D Xenes) exhibiting enhanced and complementary properties by directly moving down group IVA of the periodic table [12–16]. Among them, 2D–Germanane (2D–GeH) and its ligand-terminated 2D–Germanane (2D–GeR) derivatives have attracted increasing interest due to their semiconducting behavior, tunable band gaps, and excellent optoelectronic properties [17–19]. However, current approaches to synthesizing 2D–GeR derivatives rely on tedious topochemical reactions involving the reactivity of the $CaGe_2$ Zintl phase with organic halides (R–X) [20,21], which significantly restricts the range of functional ligands that can be incorporated. Moreover, the resulting 2D–GeR derivatives are prone to oxidation under ambient conditions owing to the chemical instability of the Ge–C bonding. These limitations have hindered the integration of supramolecular moieties onto 2D–GeH frameworks, thereby limiting their application in chiral recognition and molecular discrimination. Although different chiral 2D systems have been successfully engineered and exploited so far [22–24], the direct covalent functionalization of 2D–GeH with a carbohydrate-based host ligand (*e.g.*, R = CD) is nowadays an unexplored field.

Herein, a simple and general synthetic approach is reported to

* Corresponding author.
E-mail address: JoseMaria.Munoz@uab.cat (J. Muñoz).
[1] These authors contributed equally to this work.

https://doi.org/10.1016/j.apmt.2025.102831
Received 18 March 2025; Received in revised form 10 June 2025; Accepted 22 June 2025
Available online 27 June 2025

engineer a highly stable carbohydrate-functionalized 2D–Germanane with built-in supramolecular stereodiscrimination capabilities. For this goal, thiolated β-CD (CD-SH) was covalently anchored onto commercially available 2D–GeH *via* Ge–S bond formation, yielding a 2D–GeCD derivative with enhanced chemical stability (see Scheme 1 for illustration). As a proof-of-principle, the resulting carbohydrate-based 2D system has been explored in two stereoselective molecular recognition processes: *(1)* as a dual-mode (optical and electrochemical) system for the discrimination of tryptophan (TRP) enantiomers, and *(2)* as a cargo–release switching system for the electrochemical discrimination of azobenzene (AZO) diastereomers. Interestingly, our findings revealed that the devised 2D–GeCD exhibits a multitasking stereodiscrimination ability to effectively distinguish between both enantiomers and diastereomers by taking advantage of its anchored supramolecular macrocyclic host. This diastereoresponsive 2D system unlocks novel applications in the field of 2D–GeR derivatives, otherwise unattainable for the pristine 2D–GeH counterpart.

2. Results and discussion

2.1. Synthesis and characterization of 2D–GeCD

As illustrated in Scheme 1a, 2D–GeCD was synthesized *via* direct thiolation chemistry. Briefly, 20 mg of commercially available 2D–GeH was suspended in 10 mL of deoxygenated acetonitrile (ACN) and ultrasonicated under an Ar atmosphere for 1 h to promote material delamination and dispersion. Subsequently, the dispersion was mixed with 10 mL of a 2.5 mM CD-SH deoxygenated aqueous solution, and aged for 12 h under stirring conditions to induce nucleophilic substitution, leading to 2D–GeCD derivative. Then, the product was centrifuged, washed several times with both deionized water and ethanol, and finally dried under vacuum conditions. Finally, the 2D–GeCD sample was stored at –5 °C until further use.

The covalent functionalization of 2D–GeH with CD-SH *via* nucleophilic substitution was demonstrated using a set of characterization techniques, such as transmission electron microscopy (TEM), X-ray powder diffraction (XRD), Fourier-transform infrared spectroscopy (FTIR), X-ray photoelectron spectroscopy (XPS), and UV–vis spectroscopy. The characterization of pristine 2D–GeH was also run for comparison.

TEM images from **Fig. S1** show the typical layered structure of pristine 2D–GeH, which remains almost unaltered after material functionalization (**Fig. S2**), suggesting that the presence of the carbohydrate-based supramolecular macrocycle (*i.e.*, CD-SH) does not significantly affect the 2D skeleton. The XRD analyses revealed three characteristic peaks for both pristine 2D–GeH and functionalized 2D–GeCD, which were assigned to [002], [011], and [110] planes (see **Fig. S3**) [20]. Since the diffraction peak at low 2θ is related to the inter-layer distance between Ge sheets by following the Bragg equation [25], a slight shift in the [002] peak position from 16.3° to 16.0° was observed after the nucleophilic substitution of the pristine 2D–GeH with the CD-SH, which corresponds to a *d*-spacing distance of 5.4 Å for pristine 2D–GeH and 5.5 Å for 2D–GeCD. Next, FTIR analyses were performed using attenuated total reflection (ATR). As shown in Fig. 1a, the pristine 2D–GeH exhibited the characteristic stretching and wagging Ge–H modes located at 1985 (υGeH), 462 and 506 cm^{-1} (ωGeH). Since pristine 2D–GeH is prone to oxidation, an additional Ge–O stretching mode (υGeO) peaked at 1019 cm^{-1} was clearly identified. After functionalization, the 2D–GeCD derivative displayed the inherent fingerprint of the supramolecular moiety located at 2914, 2850, 1360, and 1162 cm^{-1}, which are attributed to the symmetric C–H, asymmetric C–H, C–H rocking, and C–O stretching vibrational modes, respectively. Further, a new contribution at 472 cm^{-1} was observed, corresponding to the new Ge–S wagging mode (ωGeS) contribution [26]. This can be seen as the first evidence of the covalent functionalization *via* Ge–S bond formation. Remarkably, the υGeO band of pristine 2D–GeH located at 1019 cm^{-1} almost disappeared after material functionalization, pointing out the passivation activity of the anchored thiol groups to preserve the chemical structure of the 2D–GeCD derivative against air oxidation [27]. To assess the long-term stability of 2D–GeCD against air oxidation, the FTIR spectrum of the sample was recorded after 12 months. As shown in **Fig. S4**, the FTIR spectra retained the characteristic peaks associated with the carbohydrate-based selector, indicating that the Ge–S bond was preserved. Nonetheless, a noticeable increase in the υGeO band was observed after 12 months, suggesting partial oxidation of the material over this extended period. Nevertheless, the intensity of the υGeO band remains significantly lower than that observed in pristine 2D–GeH, confirming the long-term passivation effect afforded by employing thiolation chemistry.

Further, XPS analyses were run in order to verify the covalent nature of molecular immobilization. **Fig. S5** displays the XPS survey spectra of pristine 2D–GeH and functionalized 2D–GeCD. While both materials exhibited two main contributions, peaked at 30 and 533 eV —assigned to Ge 3d and O 1 s, respectively—, a new peak centered at 164 eV was observed after molecular functionalization, which is attributed to the S 2p signal of CD-SH moieties. In addition, the high-resolution Ge 3d core level spectrum of pristine 2D–GeH also revealed the three fingerprint peaks at 29.2, 30.7, and 32.0 eV ascribed to the Ge–Ge, Ge–H, and Ge–O (see **Fig. S6**). Importantly, the Ge 3d core-level spectrum of 2D–GeCD (Fig. 1b) exhibited an additional binding energy contribution peaked at 27.6 eV after the CD-SH anchoring *via* thiolation chemistry, which further verifies the Ge–S bond formation. Interestingly, the ligand-exchange quantification was calculated by the total area under the curve (Auc) of the Ge–S contribution (see **Table S1**), leading to a 23 % for 2D–GeCD. Consequently, a H:S substitution ratio around 4:1 was yielded, demonstrating an efficient ligand-exchange substitution.

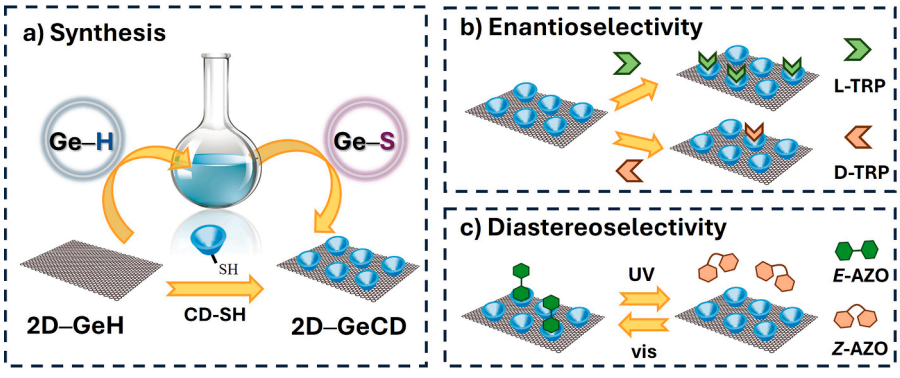

Scheme 1. Schematic illustration displaying (**a**) the synthetic procedure for the direct functionalization of 2D–GeH with CD-SH *via* thiolation chemistry. The multitasking ability of the resulting 2D–GeCD derivative was then exploited for (**b**) the enantioselectivity of TRP, and (**c**) the diastereoselectivity of AZO.

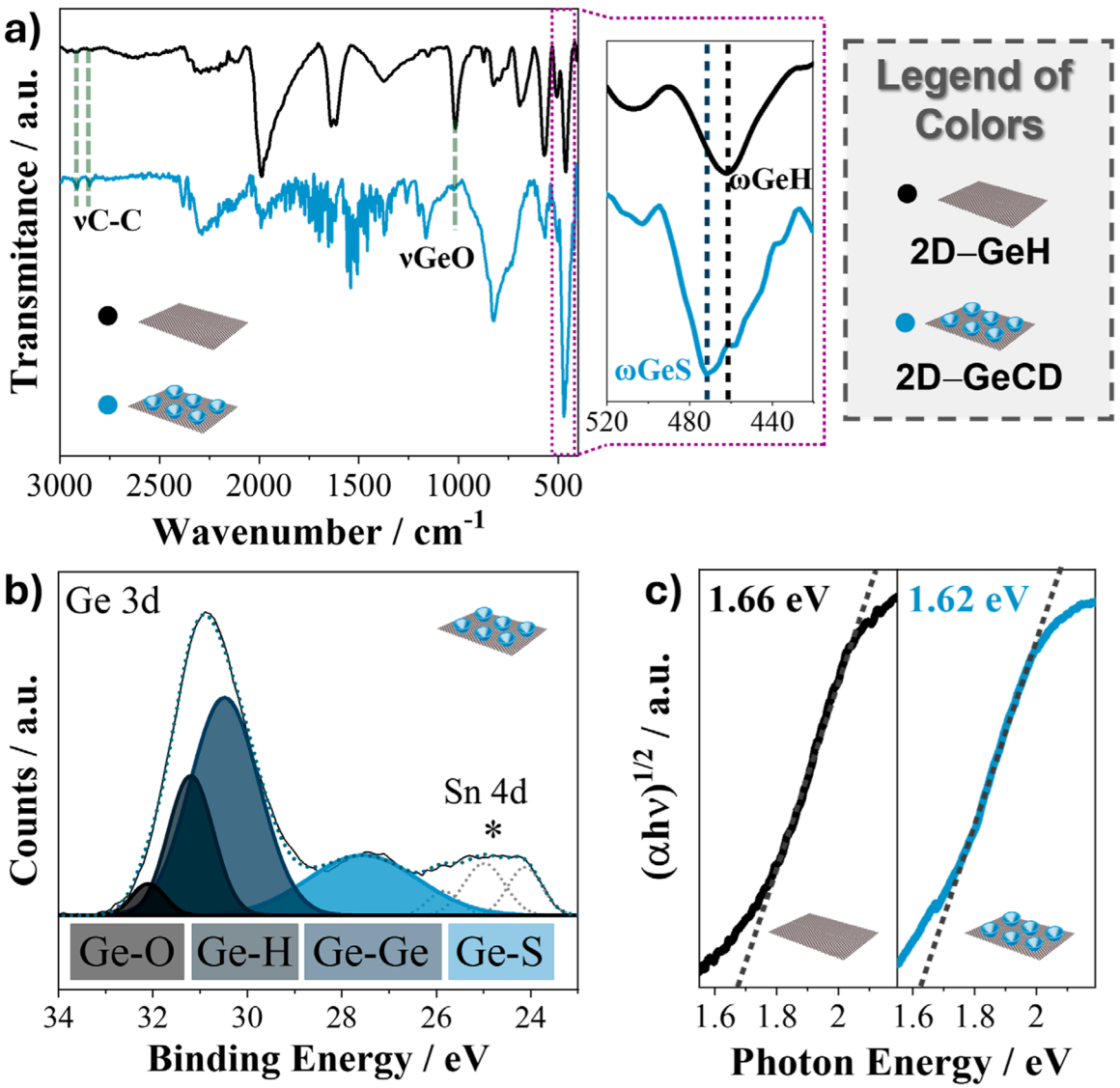

Fig. 1. Material characterization of pristine 2D–GeH and 2D–GeCD. (a) FTIR spectra (inset: enlarged region within 420–520 nm for highlighting the covalent Ge–S binding. **(b)** High-resolution core-level XPS spectrum for Ge 3d in 2D–GeCD. (*) Deconvolution peaks of Sn 4d from the fluorine-doped tin oxide (FTO) substrate. **(c)** Tauc plots with the resulting optical band gaps.

Considering that the covalent functionalization of 2D Xenes is known to modulate their optical properties, the optical bandgap of pristine 2D–GeH and functionalized 2D–GeCD was also explored. Fig. 1c displays the Tauc plots extracted from their respective UV–vis spectra (**Fig. S7**). Interestingly, a red-shift in the maximum adsorption band of pristine 2D–GeH from 603 to 623 nm was promoted after molecular functionalization, leading to a notable bandgap change from 1.66 eV for pristine 2D–GeH to 1.62 eV for 2D–GeCD. This trend is in line with our previous observations when employing alternative thiolated molecules [22]. As shown in **Fig. S8a**, the fluorescent properties were also altered after molecular functionalization, observing a significant shift in the excitation wavelength from $\lambda_{ex} = 354$ nm for pristine 2D–GeH to $\lambda_{ex} = 339$ nm for 2D–GeCD, in line with the bandgap change observed in Fig. 1c. In addition, the fluorescence intensity of pristine 2D–GeH was slightly quenched after the anchoring since thiol groups can act as hole trap states (see **Fig. S8b**).[61]

According to this accurate material characterization, it is safe to conclude at this stage that pristine 2D–GeH was successfully functionalized with the CD-SH host macrocycle *via* a ligand-exchange process, resulting in a carbohydrate-based 2D germanane derivative.

2.2. *Multitasking diastereodiscrimination ability of 2D–GeCD*

Having verified the successful synthesis of the 2D–GeCD derivatives, their multitasking diastereodiscrimination ability was evaluated by means of enantioselectivity and diastereoselectivity approaches.

Discrimination studies of TRP enantiomers with dual-mode readouts

Firstly, 2D–GeCD was explored as an unconventional chiral probe for enantioselectivity approaches, using TRP as a model chiral target (see Scheme 1b). TRP is one of many important chiral amino acids (the building blocks in protein biosynthesis), which play a pivotal role in the physiological and pharmaceutical metabolisms of biological systems [28]. For example, L-tryptophan (L-TRP) is an essential metabolite whose imbalance or deficiency may cause several chronic diseases, whereas D-tryptophan (D-TRP) is a non-protein amino acid used as an intermediate to generate synthetic peptide antibiotics and immunosuppressive agents in the pharmaceutical industry [29,30]. Consequently, the development of simple, rapid, and effective analytical methods for chiral separation and screening of active pharmaceutical ingredients (APIs) and pharmaceutical intermediates is a must. As a first demonstration of applicability, the feasibility of 2D–GeCD for the chiral

discrimination of TRP has been considered by devising a straightforward and generic dual fluorescence and electrochemical method that exploits the different host–guest binding affinity of β-CD with TRP enantiomers [31].

On the one hand, the optical enantiodiscrimination of TRP was performed using fluorescence measurements (Fig. 2). For this goal, a fixed amount of 2D–GeCD (0.025 mg mL^{-1}) in ACN was incubated with different concentrations of either L-TRP or D-TRP for 5 min under stirring conditions to induce the supramolecular host–guest complex formation. Importantly, a control experiment was also conducted with pristine 2D–GeH (see **Fig. S9**), demonstrating that no interaction between pristine 2D–GeH and chiral TRP molecules can occur in the absence of the supramolecular host component. Fig. 2a–b displays the emission spectrum (λ_{em}: 448 nm) of 2D–GeCD after incubation with increasing concentrations of L-TRP and D-TRP, respectively. Both TRP enantiomers quenched the fluorescence of 2D–GeCD since the indole group of the amino acid acts as an electron donor [32], leading to a detection limit as low as 10 nM for both chiral targets. However, as shown in the calibration curves from Fig. 2c, this quenching was found to be highly enantioselective since the photosensitivity was highly increased (50 %) for the L-TRP [note the different slope (S) values; S_L/S_D = 2.0]. Remarkably, this 50 % increase in photosensitivity is well in line with the divergent inclusion binding strength of the host β-CD with the different guest enantiomers (tabulated stability constants (log *K*): 2.33 for L-TRP *vs.* 1.11 for D-TRP) [32].

On the other hand, the electrochemical performance of 2D–GeCD towards the electrochemical oxidation of TRP enantiomers was also investigated using Linear Sweep Voltammetry (LSV). Experiments were carried out in a three-electrode configuration cell filled with a phosphate buffer solution (PBS) at pH 7.2. The enantiodiscrimination event was based on incubating the working electrode cast with 2D–GeCD with 1.0 μM TRP enantiomers for 5 min to promote supramolecular host–guest interactions, followed by its electrochemical oxidation. As shown in Fig. 3a, pristine 2D–GeH (control experiment) overlapped the voltammograms since no enantioselective recognition can occur without the presence of the chiral host. Fig. 3b presents a clear electrochemical discrimination of TRP enantiomers by means of redox potential (E_p) and peak current (I_p) when employing the carbohydrate-based 2D germanane derivative. Recognition efficiencies of 60 mV for peak-to-peak separation (ΔE_{L-D}) and 1.55 μA for peak current ratio (I_L/I_D) were estimated by LSV, which was extracted from specific E_p values at 0.93 V (I_L, green line) and 0.86 V (I_D, orange line), respectively. The difference in these pivotal electrochemical parameters implies that the 2D–GeCD can interact with L-TRP and D-TRP in different ways, as was expected from the fluorometric assay (see Fig. 2), demonstrating again that the 2D–GeCD preferentially recognizes L-TRP. This fact can be mainly attributed to a more favorable affinity of the secondary hydroxyl groups from the β–CD rims to form hydrogen bonds (H–bonds) with the amino groups of L-TRP (rather than D-TRP) when the indole group of TRP isomers inserts into the β–CD cavity [33]. Further, the ability of the 2D–GeCD to determine the enantiomeric purity of TRP was examined employing different mole fractions of L-TRP ($X_{L\text{-TRP}}$). As displayed in Fig. 3c, the E_p significantly shifted when the solution contained varying amounts of D-TRP, exhibiting a notable linear correlation curve (r^2 = 0.99, see Fig. 3d). This result demonstrates the ability of 2D–GeCD to discriminate whether the mixture is pure in L-TRP (the desired API compound) or not.

Finally, the enantioselective performance of the dual-mode 2D–GeCD system towards TRP enantiomers was compared with that of previously reported chiral 2D systems using either optical or electrochemical readouts, as summarized in **Table S2**. Remarkably, 2D–GeCD enables the possibility of not only discriminating between TRP enantiomers *via* a dual (optical and electrochemical) method but also sensing voltamperometrically the excess of D-TRP in enantiomeric mixtures. From a pharmacological point of view, this is especially appealing since 2D–GeCD might be further exploited as a rapid screening system of the pure API compound among contaminated mixtures of D-TRP.

Discrimination studies of AZO diastereomers with electrochemical readouts

Secondly, the ability of 2D–GeCD for diasteroselectivity approaches was explored. Large biomacromolecules are involved in the regulation of physiological processes and are of special interest as cargo in delivery systems [34]. In this regard, the light-driven catch and release of AZO diastereomers in β-CD has been widely exploited as a drug-delivery vehicle approach [35]. Thus, this target may serve as a suitable model molecule in the investigation of non-covalent interactions between chemical or biological species and the described 2D–GeCD [36].

The molecular basis of the photo-responsive supramolecular nanoarchitecture is the *Z–E* isomerization of the AZO molecule (see Scheme 1c for illustration). While the non-polar and straight *E*-AZO isomer forms a stable inclusion complex with β-CD, the more polar and bent *Z*–form obtained after irradiation with UV light is sterically hindered from complexation [37]. Fig. 4a–b shows the electrochemical performance of pristine 2D–GeH and 2D–GeCD loaded with 1.0 μM of AZO before and after illumination with UV light for 10 min to induce photo-isomerization. Electrochemical experiments were recorded by means of cyclic voltammetry (CV) using $[Fe(CN)_6]^{3-/4-}$ as a benchmark redox marker. The control experiment of Fig. 4a demonstrated that the electrochemical behavior of pristine 2D–GeH was not affected after inducing photo-isomerization, suggesting that no physisorption of AZO occurs on the 2D–GeH surface. On the contrary, Fig. 4b revealed two distinguishable electrochemical states on 2D–GeCD, depending on the isomeric nature of the photo-responsive AZO moiety, which was discerned by means of *Ip* (ΔIp = 80.5 μA). Such voltammetric outcomes can

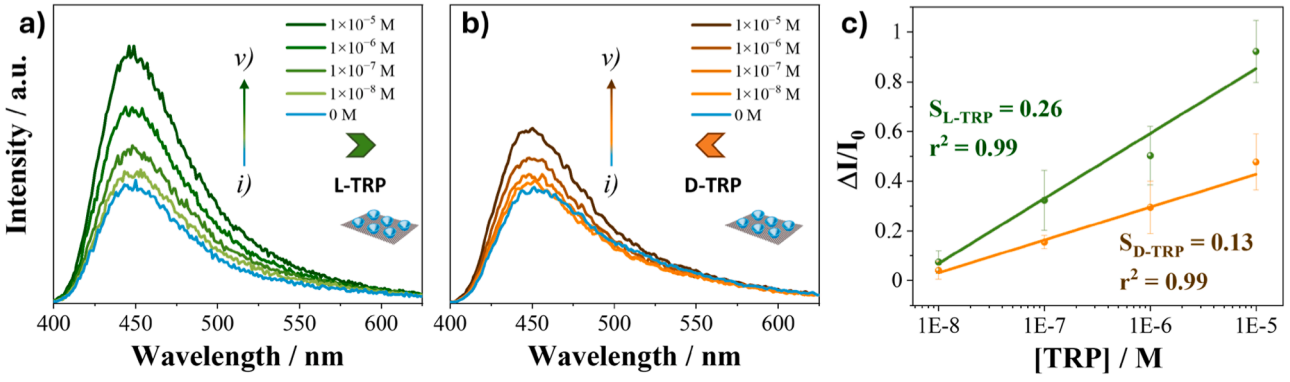

Fig. 2. Optical discrimination of TRP enantiomers. Fluorescence spectra of 2D–GeCD before and after increasing concentrations of (**a**) L-TRP and (**b**) D-TRP ([TRP]: (*i*) 0, (*ii*) $1{\cdot}10^{-8}$, (*iii*) $1{\cdot}10^{-7}$, (*iv*) $1{\cdot}10^{-6}$, and (*v*) $1{\cdot}10^{-5}$ M), with (**c**) their corresponding calibration curves. Conditions: excitation wavelength: 354 nm, incubation time: 5 min.

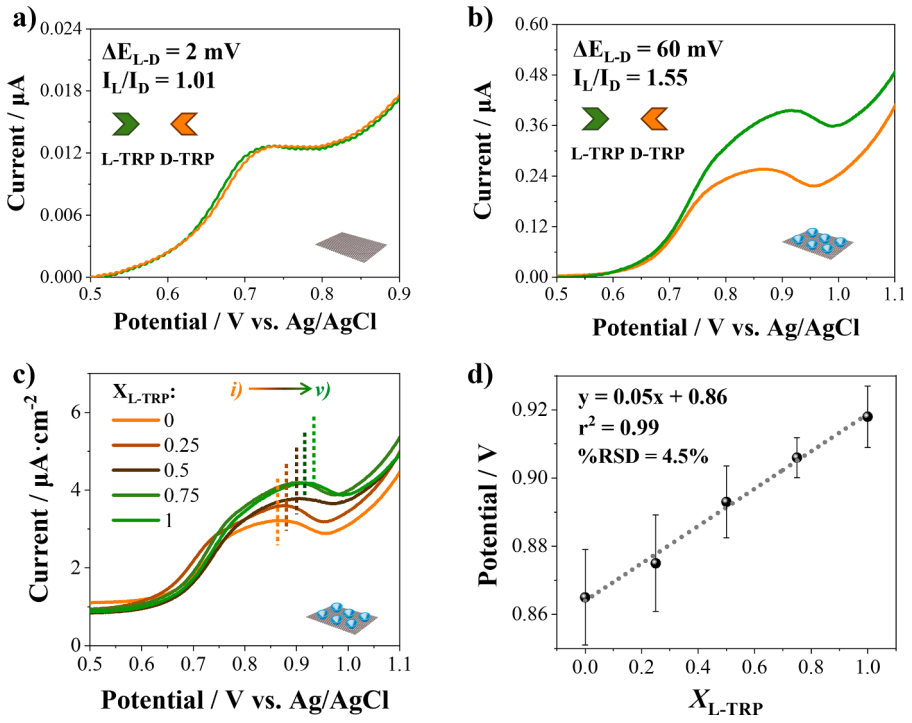

Fig. 3. Electrochemical discrimination of TRP enantiomers. LSVs after interacting with a fixed concentration of TRP enantiomers for (**a**) pristine 2D–GeH and (**b**) 2D–GeCD. (**c**) LSV of 2D–GeCD at different enantiomeric mixtures of TRP, represented as $X_{L\text{-}TRP}$ (*i*) 0, (*ii*) 0.25, (*iii*) 0.5, (*iv*) 0.75, and (*v*) 1, and (**d**) the corresponding calibration curve ($n = 3$) depicting the redox potential *vs.* the $X_{L\text{-}TRP}$. Experiments were conducted in 10 mM PBS at pH 7.2; scan rate: 20 mV·s^{-1}, incubation time: 5 min.

be accounted by changes in the interfacial electron transfer reaction at the 2D–GeCD/electrolyte interface promoted by the applied optical inputs.

On the one hand, the encapsulation of *E*-AZO onto 2D–GeCD blocks the electrode surface, thereby hindering the electron transfer reaction of the redox marker. From an electrochemical point of view, this can be translated as lower I_p (710.6 μA). Otherwise, after UV illumination, the release of the *Z*-AZO from the 2D–GeCD leads to an increase in the I_p value (791.1 μA) since the $[Fe(CN)_6]^{3-/4-}$ can penetrate easily, a fact that facilitates its interfacial electron transfer. Hence, the changes in electrochemical signal readouts must be attributed to the catch and release properties of 2D–GeCD with different AZO diastereomers. Finally, the reversibility and stability of the supramolecular switch after different UV/vis irradiation cycles were also interrogated (Fig. 4c). An ON/OFF signal ratio of 4 ± 2 % (calculated as $\%\Delta I_p$) was obtained by manipulating the light source for several cycles, demonstrating a consistent reversibility.

Lastly, to elucidate the key role of the 2D Xene platform, a control experiment was performed to evaluate the discrimination ability of isolated CD-SH toward AZO diastereomers. As shown in the CV plot from Fig. 4d, the isolated CD-SH was also capable of differentiating between the AZO isomers, yielding a $\%\Delta I_p$ of 2.6 %. However, this value is notably lower than the 4 % obtained with 2D–GeCD. This reduced ON/OFF ratio might be ascribed to the random spatial orientation of the isolated CD-SH through the electrode surface, which likely limits the accessibility of its cavities for effective supramolecular host–guest interactions with the AZO target. These findings demonstrate the pivotal role of the 2D Xene scaffold in aligning the supramolecular selector to enhance supramolecular recognition efficiency.

The above results demonstrate not only the suitability of 2D–GeCD to discriminate between AZO diastereomers, but also envision its ability to act as a cargo vehicle for drug delivery.

3. Conclusions

In summary, an unprecedented carbohydrate-based 2D germanane derivative with built-in stereodiscrimination ability has been successfully synthesized through the direct functionalization of pristine 2D–GeH with CD-SH *via* thiolation chemistry. After an accurate material characterization, the implanted supramolecular features of the carbohydrate-based host selector have been shown to be retained in the resulting 2D–GeCD structure, while demonstrating the enhanced chemical stability of the 2D system *via* Ge–S bond formation. By employing supramolecular host–guest chemistry, the multitasking ability of 2D–GeCD derivatives has been exploited not only for the discrimination of TRP enantiomers but also AZO diastereomers. In addition, the output signals of the stereorecognition system have been read out by means of optical and/or electrochemical analyses, pointing out the versatility of the approach.

Consequently, the reported methodology, which might be simply customized by tailoring the host–guest system, demonstrates the suitability of combining 2D–GeH with carbohydrate-based host selectors to expand the family, functionality, stability, and implementation of emerging 2D Xenes in yet unexplored fields, otherwise unattained for the pristine counterparts.

The Supporting Information is available free of charge and contains details of experiments and methods, additional characterization techniques (TEM images, additional spectroscopic techniques, and control tests), and supplementary figures and tables.

CRediT authorship contribution statement

Yiming Lei: Writing – review & editing, Methodology, Investigation, Formal analysis. **Ángel Campos-Lendínez:** Writing – review & editing, Methodology, Investigation, Formal analysis, Data curation. **Xavier Sala:** Writing – review & editing, Resources, Funding acquisition. **Jordi García-Antón:** Writing – review & editing, Supervision, Resources,

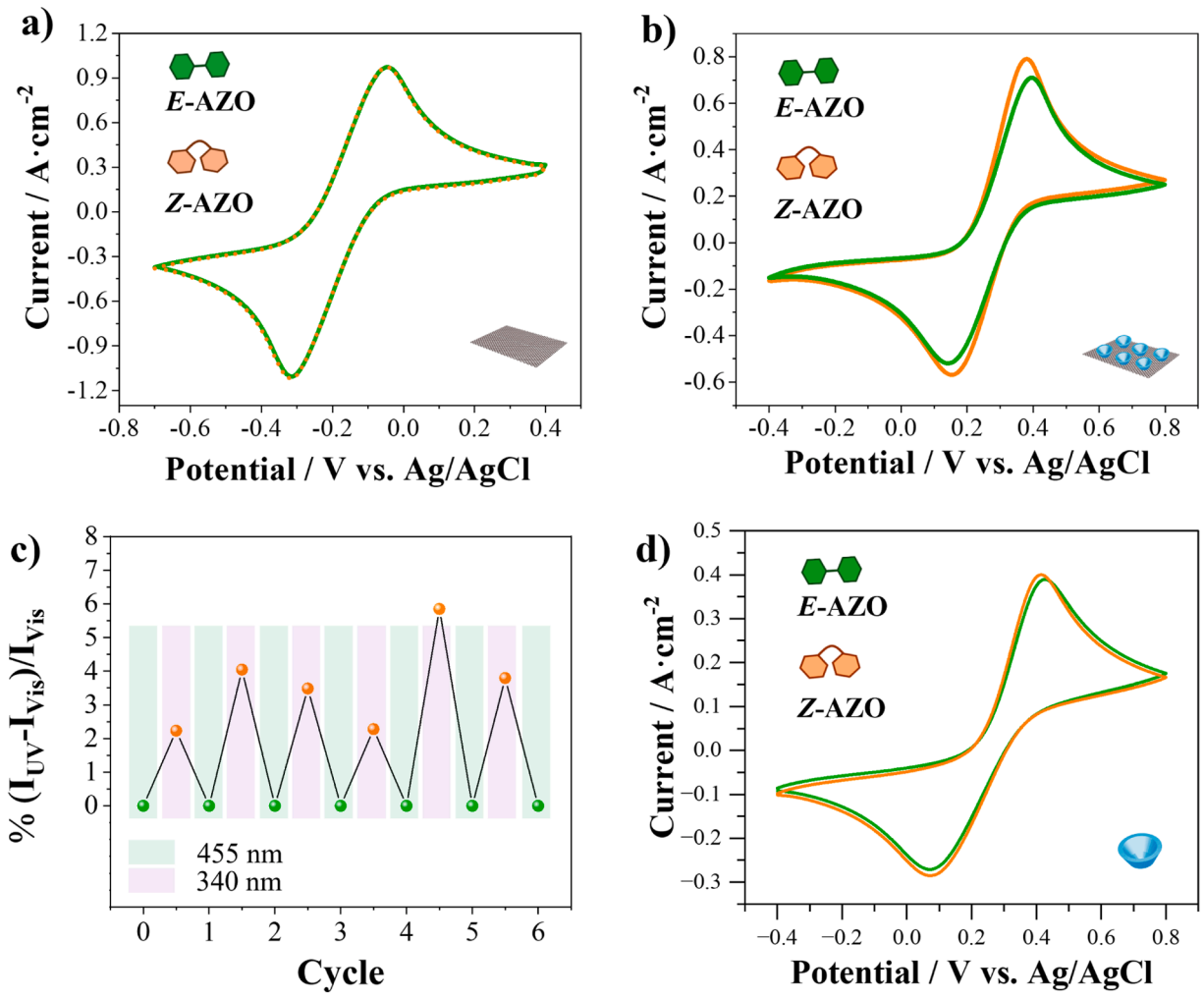

Fig. 4. Electrochemical discrimination of AZO diastereoisomers. CV of (**a**) pristine 2D–GeH and (**b**) 2D–GeCD before (*E*-AZO) and after irradiating with UV light (*Z*-AZO). (**c**) Cyclability of the light-driven molecular switch achieved at the 2D–GeCD surface by modulating the light source (visible light *vs.* UV light). (**d**) CV of isolated CD-SH (control experiment) before (*E*-AZO) and after irradiating with UV light (*Z*-AZO). Experiments were conducted in 0.1 M KCl containing 10 mM $[Fe(CN)_6]^{3-/4-}$; scan rate: 100 $mV{\cdot}s^{-1}$; irradiation period and incubation time: 10 min.

Funding acquisition. **Jose Muñoz:** Writing – review & editing, Writing – original draft, Supervision, Resources, Conceptualization.

Declaration of competing interest

The authors declare the following financial interests/personal relationships which may be considered as potential competing interests: Jose Munoz reports financial support was provided by Autonomous University of Barcelona. If there are other authors, they declare that they have no known competing financial interests or personal relationships that could have appeared to influence the work reported in this paper.

Acknowledgments

Y. L. and A. C-L. contributed equally to this work. Y. L. acknowledges the program of the China Scholarships Council (No. 202206250016). X. S. thanks ICREA for the ICREA Academia Prize 2020. J. M. is indebted to the Ramón y Cajal Program (RYC2021–033820-I Fellowship) funded by MCIN/AEI/10.13039/501100011033 and by the European Union "NextGenerationEU/PRTR". The authors thank MICINN (PID2023–146787OB-I00) and AGAUR (2024-PROD-00046) for financial support.

Supplementary materials

Supplementary material associated with this article can be found, in the online version, at doi:10.1016/j.apmt.2025.102831.

Data availability

Data will be made available on request.

References

[1] M. González-Cuesta, C. Ortiz Mellet, J.M. García Fernández, Carbohydrate supramolecular chemistry: beyond the multivalent effect, Chem. Commun. 56 (2020) 5207–5222, https://doi.org/10.1039/D0CC01135E.
[2] A. Mittal, Krishna, Aarti, S. Prasad, P.K. Mishra, S.K. Sharma, B. Parshad, Self-assembly of carbohydrate-based small amphiphiles and their applications in pathogen inhibition and drug delivery: a review, Mater. Adv. 2 (2021) 3459–3473, https://doi.org/10.1039/D0MA00916D.
[3] M.A. Khalilzadeh, S.Y. Kim, H.W. Jang, R. Luque, R.S. Varma, R.A. Venditti, M. Shokouhimehr, Carbohydrate-based nanostructured catalysts: applications in organic transformations, Mater. Today Chem. 24 (2022) 100869, https://doi.org/10.1016/j.mtchem.2022.100869.
[4] L. Su, Y. Feng, K. Wei, X. Xu, R. Liu, G. Chen, Carbohydrate-based macromolecular biomaterials, Chem. Rev. 121 (2021) 10950–11029, https://doi.org/10.1021/acs.chemrev.0c01338.
[5] S. Gim, Y. Zhu, P.H. Seeberger, M. Delbianco, Carbohydrate-based nanomaterials for biomedical applications, WIREs Nanomed. Nanobiotechnol. 11 (2019), https://doi.org/10.1002/wnan.1558.

[6] S. Penadés (Ed.), Host-Guest Chemistry, Springer, Berlin Heidelberg, Berlin, Heidelberg, 2002, https://doi.org/10.1007/3-540-45010-6.
[7] J. Muñoz, N. Crivillers, B.J. Ravoo, M. Mas-Torrent, Cyclodextrin-based superparamagnetic host vesicles as ultrasensitive nanobiocarriers for electrosensing, Nanoscale 12 (2020) 9884–9889, https://doi.org/10.1039/D0NR01702G.
[8] J. Muñoz, E. Redondo, M. Pumera, Bistable (Supra)molecular switches on 3D-printed responsive interfaces with electrical readout, ACS Appl. Mater. Interfaces 13 (2021) 12649–12655, https://doi.org/10.1021/acsami.0c14487.
[9] J. Muñoz, M. Riba-Moliner, L.J. Brennan, Y.K. Gun'ko, F. Céspedes, A. González-Campo, M. Baeza, Amperometric thyroxine sensor using a nanocomposite based on graphene modified with gold nanoparticles carrying a thiolated β-cyclodextrin, Microchim. Acta 183 (2016) 1579–1589, https://doi.org/10.1007/s00604-016-1783-x.
[10] L. Karadurmus, M. Gumustas, N.K. Bakirhan, S.A. Ozkan, Chiral sensing as a future challenge in electroanalytical chemistry: cyclodextrin-based Chiral sensors, Crit. Rev. Anal. Chem. 53 (2023) 498–519, https://doi.org/10.1080/10408347.2021.1967108.
[11] J. Zhang, P.X. Ma, Cyclodextrin-based supramolecular systems for drug delivery: recent progress and future perspective, Adv. Drug Deliv. Rev. 65 (2013) 1215–1233, https://doi.org/10.1016/j.addr.2013.05.001.
[12] A. Molle, C. Grazianetti, L. Tao, D. Taneja, M.H. Alam, D. Akinwande, Silicene, silicene derivatives, and their device applications, Chem. Soc. Rev. 47 (2018) 6370–6387, https://doi.org/10.1039/C8CS00338F.
[13] J. Muñoz, Rational design of stimuli-responsive inorganic 2D materials via molecular engineering: toward molecule-programmable nanoelectronics, Adv. Mater. 36 (2024) 2305546, https://doi.org/10.1002/adma.202305546.
[14] J. Muñoz, M. Palacios-Corella, I.J. Gómez, L. Zajíčková, M. Pumera, Synthetic nanoarchitectonics of functional organic–inorganic 2D germanane heterostructures via click chemistry, Adv. Mater. 34 (2022), https://doi.org/10.1002/adma.202206382.
[15] J. Luxa, P. Vosecký, V. Mazánek, D. Sedmidubský, M. Pumera, Z. Sofer, Cation-controlled electrocatalytical activity of transition-metal disulfides, ACS Catal. 8 (2018) 2774–2781, https://doi.org/10.1021/ACSCATAL.7B04233/SUPPL_FILE/CS7B04233_SI_001.PDF.
[16] J. Luxa, V. Mazánek, D. Bouša, D. Sedmidubský, M. Pumera, Z. Sofer, Graphene–Amorphous transition-metal chalcogenide (MoSx, WSx) composites as highly efficient hybrid electrocatalysts for the hydrogen evolution reaction, ChemElectroChem 3 (2016) 565–571, https://doi.org/10.1002/CELC.201500497.
[17] T. Hartman, Z. Sofer, Beyond graphene: chemistry of group 14 graphene analogues: silicene, germanene, and stanene, ACS Nano 13 (2019) 8566–8576, https://doi.org/10.1021/acsnano.9b04466.
[18] S. Balendhran, S. Walia, H. Nili, S. Sriram, M. Bhaskaran, Elemental analogues of graphene: silicene, germanene, stanene, and phosphorene, Small 11 (2015) 640–652, https://doi.org/10.1002/SMLL.201402041.
[19] S. Balendhran, S. Walia, H. Nili, S. Sriram, M. Bhaskaran, The development of two dimensional group IV chalcogenides, blocks for van der Waals heterostructures, Nanoscale 8 (2015) 1169–1178, https://doi.org/10.1039/C5NR06871A.
[20] S. Jiang, S. Butler, E. Bianco, O.D. Restrepo, W. Windl, J.E. Goldberger, Improving the stability and optical properties of germanane via one-step covalent methyl-termination, Nat. Commun. 5 (2014) 3389, https://doi.org/10.1038/ncomms4389.
[21] S. Jiang, K. Krymowski, T. Asel, M.Q. Arguilla, N.D. Cultrara, E. Yanchenko, X. Yang, L.J. Brillson, W. Windl, J.E. Goldberger, Tailoring the electronic structure of covalently functionalized germanane via the interplay of ligand strain and electronegativity, Chem. Mater. 28 (2016) 8071–8077, https://doi.org/10.1021/acs.chemmater.6b04309.
[22] J. Muñoz, A. González-Campo, M. Riba-Moliner, M. Baeza, M. Mas-Torrent, Chiral magnetic-nanobiofluids for rapid electrochemical screening of enantiomers at a magneto nanocomposite graphene-paste electrode, Biosens. Bioelectron. 105 (2018) 95–102, https://doi.org/10.1016/j.bios.2018.01.024.
[23] S. Gim, G. Fittolani, Y. Nishiyama, P.H. Seeberger, Y. Ogawa, M. Delbianco, Supramolecular assembly and chirality of synthetic carbohydrate materials, Angew. Chem. Int. Ed. 59 (2020) 22577–22583, https://doi.org/10.1002/anie.202008153.
[24] M.B. Avinash, T. Govindaraju, Nanoarchitectonics of biomolecular assemblies for functional applications, Nanoscale 6 (2014) 13348–13369, https://doi.org/10.1039/C4NR04340E.
[25] T. Hartman, J. Sturala, J. Plutnar, Z. Sofer, Alkali metal arenides as a universal synthetic tool for layered 2D germanene modification, Angew. Chem. Int. Ed. 58 (2019) 16517–16522, https://doi.org/10.1002/anie.201910654.
[26] Á. Campos-Lendinez, J. Faraudo, J. García-Antón, X. Sala, J. Muñoz, Direct covalent functionalization of H-terminated 2D germanane with thiolated molecules: passivation and tuning of optoelectronic properties, ACS Appl. Mater. Interfaces (2024), https://doi.org/10.1021/acsami.4c17152.
[27] G. Collins, D. Aureau, J.D. Holmes, A. Etcheberry, C. O'Dwyer, Germanium oxide removal by citric acid and thiol passivation from citric acid-terminated Ge(100), Langmuir 30 (2014) 14123–14127, https://doi.org/10.1021/la503819z.
[28] C. Buten, L. Kortekaas, B.J. Ravoo, Design of active interfaces using responsive molecular components, Adv. Mater. 32 (2020) 1904957, https://doi.org/10.1002/adma.201904957.
[29] L. Chen, Y. Chen, Y. Zhang, Y. Liu, Photo-controllable catalysis and chiral monosaccharide recognition induced by cyclodextrin derivatives, Angew. Chem. Int. Ed. 60 (2021) 7654–7658, https://doi.org/10.1002/anie.202017001.
[30] I. Tomatsu, A. Hashidzume, A. Harada, Contrast viscosity changes upon photoirradiation for mixtures of poly(acrylic acid)-based α-cyclodextrin and azobenzene polymers, J. Am. Chem. Soc. 128 (2006) 2226–2227, https://doi.org/10.1021/ja058345a.
[31] T. Li, Y. Wang, X. Kan, Electrochemical chiral recognition of tryptophan enantiomers based on copper-modified β-cyclodextrin, J. Electroanal. Chem. 902 (2021) 115817, https://doi.org/10.1016/j.jelechem.2021.115817.
[32] C. Han, H. Li, Chiral recognition of amino acids based on cyclodextrin-capped quantum dots, Small 4 (2008) 1344–1350, https://doi.org/10.1002/SMLL.200701221.
[33] J. Muñoz, M. Urso, M. Pumera, Self-propelled multifunctional microrobots harboring chiral supramolecular selectors for "enantiorecognition-on-the-fly, Angew. Chem. Int. Ed. 61 (2022) e202116090, https://doi.org/10.1002/ANIE.202116090.
[34] L. Stricker, E.-C. Fritz, M. Peterlechner, N.L. Doltsinis, B.J. Ravoo, Arylazopyrazoles as light-responsive molecular switches in cyclodextrin-based supramolecular systems, J. Am. Chem. Soc. 138 (2016) 4547–4554, https://doi.org/10.1021/jacs.6b00484.
[35] Y. Wang, N. Ma, Z. Wang, X. Zhang, Photocontrolled reversible supramolecular assemblies of an azobenzene-containing surfactant with α-cyclodextrin, Angew. Chem. Int. Ed. 46 (2007) 2823–2826, https://doi.org/10.1002/anie.200604982.
[36] S.K.M. Nalluri, B.J. Ravoo, Light-responsive molecular recognition and adhesion of vesicles, Angew. Chem. Int. Ed. 49 (2010) 5371–5374, https://doi.org/10.1002/anie.201001442.
[37] J. Blass, B.L. Bozna, M. Albrecht, J.A. Krings, B.J. Ravoo, G. Wenz, R. Bennewitz, Switching adhesion and friction by light using photosensitive guest–host interactions, Chem. Commun. 51 (2015) 1830–1833, https://doi.org/10.1039/C4CC09204J.